Photophysical and electron attachment properties of ArF-excimer-laser irradiated H_2

Panos G. Datskos and Lal A. Pinnaduwage
Health Sciences Research Division, Oak Ridge National Laboratory, P.O. Box 2008, Oak Ridge, Tennessee 37831-6122
and Department of Physics and Astronomy, University of Tennessee, Knoxville, Tennessee 37996-1200

John F. Kielkopf
Department of Physics, University of Louisville, Louisville, Kentucky 40292
(Received 14 November 1996; revised manuscript received 23 January 1997)

Detailed electron attachment and spectroscopic measurements are reported on ArF-excimer-laser irradiated H_2. These studies indicate that previously reported efficient H^- formation in ArF-laser irradiated H_2 is due to electron attachment to high-lying Rydberg (HR) states indirectly populated by the laser irradiation. Electron attachment studies indicate a lifetime of $\geqslant 40$ ns for the electron attaching state(s). The spectroscopic studies show that vacuum ultraviolet emission due to the $B\ ^1\Sigma_u^+ \rightarrow X\ ^1\Sigma_g^+$ transitions continues for up to ~ 100 ns after the termination of the laser pulse and thus that the B state is populated by cascades from higher-lying states with longer lifetimes. The temporal profile of Lyman-α emission due to the H($n=2$) to H($n=1$) transitions is consistent with the production of H($n=2$) states by electron attachment to HR states. [S1050-2947(97)00206-0]

PACS number(s): 33.20.−t, 33.80.−b, 34.10.+x, 32.80.Rm

I. INTRODUCTION

Electron attachment to the $v=0$ vibrational level of ground electronic state $X\ ^1\Sigma_g^+$, of H_2 molecules (where most of the H_2 molecules are at 300 K) is extremely weak, having a peak cross section of $\sim 1.6\times 10^{-21}$ cm^2 at an electron energy of 3.75 eV (rate constant $\sim 10^{-14}$ cm^3 s^{-1}) [1]. However, the electron attachment cross section was shown to increase rapidly with increasing vibrational energy, and an enhancement of more than four orders of magnitude was observed for the $v=4$ level [2,3]. Subsequent extended calculations [4,5] showed that the maximum electron attachment rate constant for the higher-vibrational states approached a maximum value of $\sim 10^{-8}$ cm^3 s^{-1} around $v=8$. The electron attachment cross section for the metastable $c\ ^3\Pi_u$ state was calculated [6] to be $\sim 10^{-18}$ cm^2, an enhancement of about three orders compared to the $v=0$ level of the $X\ ^1\Sigma_g^+$.

In 1993 experimental evidence was presented [7] to show that an extremely efficient electron attachment process was involved in ArF-excimer-laser-irradiated H_2; an absolute lower limit of 10^{-6} cm^3 s^{-1} was estimated [7] for the electron attachment rate constant involved. Subsequently, photodetachment and ion mobility measurements were conducted [8] to verify H^- formation by the above process. The high efficiency with which H^- ions are populated in ArF-laser-excited H_2 was illustrated in an independent experiment: Kielkopf [9] had observed laser emission in aluminum when Al was irradiated by the ArF laser in the presence of H_2. Recently it was shown [10] that efficient H^- formation by electron attachment to ArF-laser-excited H_2 was responsible for the charge neutralization of Al^+ that led to the population of the lasing Al state. Lasing in Al was observed within a few ns following the ArF pulse; therefore, H^- formation must have been completed well within that time.

A schematic potential energy diagram for H_2 is shown in Fig. 1. The potential energy curves for the electronic states shown were taken from Sharp [11] except for the doubly excited superexcited state $^1\Sigma_u^+(2p\sigma_u\,2s\sigma_g)$, which was taken from Guberman [12]. The absorption of two photons of the 193 nm ArF-excimer line results in the excitation of H_2 from its ground state $X\ ^1\Sigma_g^+(v=0)$ to the $E,F\ ^1\Sigma_g^+(v=6)$ level (this vibrational state is sometimes labeled as $v_e=2$, referring to the level located in the inner potential well E of the double-minimum state), i.e.,

$$H_2(X\ ^1\Sigma_g^+)(v=0)+2h\nu(\lambda=193\ \text{nm}) \rightarrow H_2^*(E,F\ ^1\Sigma_g^+)(v=6). \quad (1)$$

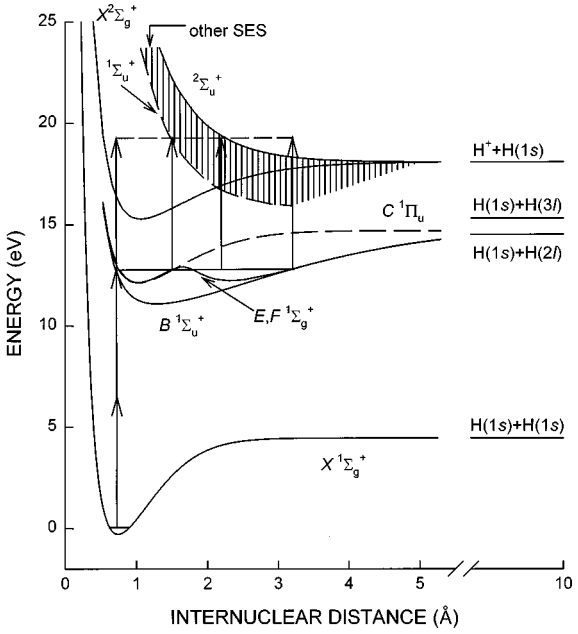

FIG. 1. Schematic energy level diagram of the H_2 molecule showing the states of relevance to the discussion in the text [11,12]. There are seven singlet SES states that lie in the shaded area between the $^1\Sigma^+$ and the $^2\Sigma^+$ states [12].

The two-photon excitation cross section for the transition from the $X\ ^1\Sigma_g^+$ to the double well $E,F\ ^1\Sigma_g^+$ has been reported [13] to be $\sim 10^{-47}$ cm^4 s^{-1}; this value was shown to be in reasonable agreement with a calculation [14] after a simple correction was made [13]. Even though the Franck-Condon region for the $X\ ^1\Sigma_g^+ \rightarrow E,F\ ^1\Sigma_g^+$ transition is restricted to the inner E well of the double-minimum state (see Fig. 1), both wells are populated due to the efficient tunneling especially for the $v=6$ state lying close to the top of the barrier [15–17]. Therefore, further photoexcitation from the intermediate E,F states takes place from both E and F wells over a large range of internuclear distance (see Fig. 1), and has been shown to be quite efficient [13,18]. Photon absorption from the E,F level can lead to the following outcomes: (i) direct ionization,

$$H_2^*(E,F)+h\nu \rightarrow H_2^+ + e^-(H+H^+ + e^-) \qquad (2)$$

and (ii) population of a series composed of doubly excited superexcited states (SES) [12] converging to the $^2\Sigma_u^+$ excited ion state (in the hatched region of Fig. 1),

$$H_2^*(E,F)h\nu \rightarrow H_2^{**}. \qquad (3)$$

The radiative lifetime of the $E,F\ ^1\Sigma_g^+(v=6)$ has been measured [18–20] to be ~ 100 ns. Fluorescence emission from ArF-laser irradiated H_2 has been analyzed by several groups [13,18,19,21,22]. In all these experiments, commercial ArF lasers with pulse durations full width at half maximum (FWHM) of ~ 20 ns were employed, except in the case of Pummer *et al.* [21] who used a tunable ps ArF laser. Kligler and co-workers [18,19] measured the quenching of the E,F states by collisions with ground-state H_2 molecules by monitoring the near-infrared emission from the E well to the $B\ ^1\Sigma_u^+(v=0$ and $v=1)$ levels; they reported a collisional deactivation rate constant of $\sim 2.1\times 10^{-9}$ cm^3 s^{-1}, which was confirmed by Buck *et al.* [13] using similar measurements. This deactivation was proposed [18] to be due to population transfer to the nearly degenerate $C(v=2)$ state, see Fig. 1. Since the E and F wells are strongly coupled [15–17] for vibrational states close to the top of the barrier (in this case the $v=6$ and $v=5,7$ levels located, respectively, in the E and F wells), the collisional deactivation reduces the lifetime of the populations in both wells. (To our knowledge, the emission due to $F \rightarrow B$ transitions that lie in the IR range at ~ 2.5 μm has not been reported.) Using the collisional deactivation rate constant of $\sim 2.1 \times 10^{-9}$ cm^3 s^{-1}, it can be seen that at the H_2 pressures of 5–50 Torr used in the present experiments, the effective lifetime of the E,F state ranged from ~ 3 to ~ 0.3 ns.

In addition to the near-IR emission from the direct $E \rightarrow B$ transitions discussed above, vacuum-ultraviolet (VUV) emission has been observed from ArF-laser irradiated H_2 due to the Lyman band $B \rightarrow X$ transitions [18,21] and the Werner band $C \rightarrow X$ transitions [18,21,22]. The B state may be populated by $E,F \rightarrow B$ radiative transitions and the C state may be populated by collisions of the E state with ground-state H_2 molecules [18] or with electrons [21]. The electron collisional rate constant is estimated [23,24] to be $\sim 7 \times 10^{-6}$ cm^3 s^{-1} and thus is negligible at electron densities $< 10^{10}$ cm^{-3} involved in the present experiments; hence, collisions with ground-state H_2 molecules seem to be responsible for the population of C state under our experimental conditions. The radiative lifetimes of the B [25] and C [26] states are each ~ 0.6 ns.

In addition to the B-X and C-X transitions, we have observed Lyman-α emission due to H($n=2$) to H($n=1$) transitions. At low spectral resolution this emission overlaps the C-X emission, but its characteristic narrow spike at 1215 Å was unmistakable in our experiments.

A. Candidate species for H^- formation in ArF-laser irradiated H_2

From the above discussion an inference can be made that the electron attaching species responsible for the observed [7,8] H^- formation could be due to a variety of species that have their origins in various products due to laser irradiation. In the following we will summarize these and discuss their possible role in the observed H^- formation.

1. Possible mechanisms with origins in the E,F state

The excitation of the $E,F\ ^1\Sigma_g^+(v=6)$ state by two-photon absorption from the ground state [see, Eq. (1)] leads to the following possibilities for the electron attaching species: (i) the E,F vibrational states directly populated by two-photon absorption, (ii) C vibrational states (produced by neutral collisions with the E,F states), (iii) low-vibrational states of B populated by radiative decay from the E,F states, and (iv) high-vibrational states of the ground-state X produced by $E,F \rightarrow B \rightarrow X$ cascades. In Sec. II, we present experimental measurements to show that electron attachment to the attaching species continue for ~ 40 ns after the laser pulse is turned off. This rules out (ii) and (iii) above as attaching species since their lifetimes are sub-ns [25,26]. Our experiments were carried out in the H_2 pressure range of 5–50 Torr, where the E,F state lifetime will be in the range of 3–0.3 ns [13,18,19]; thus, (i) above also can be ruled out as the attaching state. On the other hand, the observed lifetimes $\geqslant 40$ ns for the attaching state may be too short for the vibrational states of the ground X state. The radiative lifetime of the vibrational levels are $\sim 10^5$ s, but collisional vibrational relaxation reduces this lifetime; from the shock tube data of Kieffer and Lutz [27] we infer a lifetime of ~ 96 μs for vibrationally excited H_2 at 1100 K and at 50 Torr. It was also shown [7] that even though the high-vibrational states can have electron attachment rate constants up to 10^{-8} cm^3 s^{-1}, those values were too small to explain the observed H^- densities. Further evidence to rule out all the above possibilities, (i) through (iv) above, will be presented in Sec. III.

2. Possible mechanisms with their origins in the H_2^+ ion

The number density of H_2^+ ions (and electrons) will be second only to the E,F states. The H_2^+ ions are expected to be converted to H_3^+ ions rapidly [28,29]; the reaction

$$H_2^+ + H_2 \rightarrow H_3^+ + H \qquad (4)$$

has been shown [29] to have a peak cross section of $\sim 8 \times 10^{-15}$ cm^2 at thermal ion energies. Therefore, the possibility exists that H^- ions may be produced by electron collisions with either the H_2^+ or the H_3^+ ions.

Peart and Dolder [30] measured the cross section for the reaction

$$H_2^+ + e^- \rightarrow H^+ + H^- \tag{5}$$

and reported that it decreased from 4.9×10^{-18} cm^2 at 0.4 eV to 1.16×10^{-18} cm^2 at 4.96 eV electron energy.

The cross section for the production of H^- ions by electron collisions with H_3^+ ions (in the zero-vibrational level) was also measured in the electron energy range of 2–13 eV by Peart, Forest, and Dolder [31] and was reported to have a maximum of 1.6×10^{-18} cm^2 at 8 eV.

In both of the above cases [30,31], the electron energies used were in the range of electron energies in the present experiments. The above cross sections are too small to explain the efficient H^- observed in our experiments, see Sec. III. (It must be noted, however, that the H_2^+ ions produced via preionization of the SES in our experiments can have high vibrational energies. The dependence of vibrational excitation of H_2^+ and H_3^+ on the above processes has not been studied.)

3. Possible mechanisms with origins in the SES

The remaining possibilities originate from the SES, see Eq. (3). The SES themselves can be ruled out as possible attachers due to their extremely short lifetimes, of the order of 10^{-14} s [32]. The SES may decay by several different channels:

$$H_2^{**} \rightarrow \begin{cases} H_2^+ + e^- \quad \text{(autoionization)} & \text{(6a)} \\ H + H^*(n) \quad \text{(dissociation)} & \text{(6b)} \\ H^+ + H^- \quad \text{(ion-pair formation)} & \text{(6c)} \\ H_2^*(\text{HR}) \quad \text{(high Rydberg formation).} & \text{(6d)} \end{cases}$$

The ion-pair formation in Eq. (6c) has been shown to be a weak process [33]: Pratt *et al.* [33] have studied the field dependence of the threshold for ion-pair formation in H_2 in a two-laser experiment where the first laser (wavelength ~ 193 nm) populated the $E,F(v=6)$ state. In these experiments, the H^- signal due to ion-pair formation was much weaker than the H_2^+ signal due to photoionization (in contrast to the present experiments where the H^- signal can be comparable to the positive ion signal); they did not see the H^- signal with only the 193-nm laser [34]. It must be noted that their experiments were conducted under low-pressure conditions (pressure $\sim 10^{-3}$ Torr), and with narrow-band excitation with small laser pulse energies of $<100\ \mu$J [34]. Furthermore, in the present experiments, negative ions are produced via an electron attachment process, see Sec. III.

There are two possibilities for H^- formation via $H^*(n)$ atoms produced by Eq. 6(b) above. One is the reaction between two $H^*(n)$ atoms producing H^- and H^+; an analogous process involving $Na^*(n)$ has been shown [35] to have a rate constant of $\sim 10^{-7}$ cm^3 s^{-1}. However, this process does not involve the formation of negative ions at the expense of electrons (see Sec. III) and hence can be ruled out. The second possibility is electron attachment to $H^*(n)$ atoms. To our knowledge, no data exist on this process; however, radiative attachment of an electron to an unexcited H atom has been shown [36] to be weak with a cross section of $\sim 6 \times 10^{-24}$ cm^2.

All previous and present experimental evidence support the remaining possibility, i.e., electron attachment to the high Rydberg (HR) states of H_2 (which presumably lie close to the ionization threshold) populated by Eq. 6(d) above,

$$H_2^*(\text{HR}) + e^- \rightarrow H^- + H(n=2), \tag{7}$$

where n is the principal quantum number. With a value of 4.48 eV [37] for the dissociation energy of the H_2 molecule, and a value of 0.75 eV [36] for the electron affinity of H, production of a H $(n=2)$ state is energetically possible by attachment of a thermal electron to a state of H_2 with a minimum energy of ~ 14 eV.

These HR states may be populated at curve crossings at nuclear distances beyond the ''stability point'' [38,39], i.e., the intersection of the potential curves for SES with that for the $X\ ^2\Sigma_g^+$ ground state of the H_2^+ ion in the vicinity of 2.4 Å internuclear separation (see Fig. 1). Depending on the outcome of the curve crossings, formation of the HR states or dissociation into neutral fragments will occur, Eqs. 6(d) and 6(b) above, respectively. The presence of ''near-zero-energy electrons'' [40,41] in photoionization of many molecules has been attributed to the rotational or vibrational autoionization or field ionization of such HR states [38–41]. In the present case, such HR states that may be populated are likely to dissociate rapidly since their total energy lies above the dissociation threshold (see Fig. 1), unless the excess energy is removed by radiation or collisions. Radiative relaxation is probably too slow since it normally occurs in ns times. At our pressures, normal ground-state H_2-H_2 collisions occur in μs times, but in the present case we are dealing with collisions involving highly excited states. Cross sections for n-changing and l (angular momentum) changing collisions of atomic Rydberg states with neutrals are known to be characteristically large [42]. It may be speculated that the ''extra'' energy (energy above the ionization threshold) of a superexcited state may be transferred to the vibrational motion of the colliding ground-state molecules; the high density of final Rydberg states located close to the ionization threshold may lead to extremely large cross section for such a collision process.

To our knowledge, the time dependence of the $B \rightarrow X$ and $C \rightarrow X$ transitions in ArF-laser irradiated H_2 has not been measured up to now. We observe emissions from these two states for tens of ns after the ArF laser pulse is turned off (with $B \rightarrow X$ emission prevailing for >100 ns), even though the radiative lifetimes of the B and C states are ~ 0.6 ns, see Sec. III. We attribute this to the repopulation of the B and C states by cascades from higher-lying, longer-lived states that are indirectly populated by the ArF laser. This corroborates our contention [43] that such high Rydberg states are responsible for the observed electron attachment. Furthermore, we observe Lyman-α emission due to H $(n=2)$ to H $(n=1)$ transitions that also continue for up to 100 ns in spite of the fact that the H $(n=2)$ level has a mean radiative

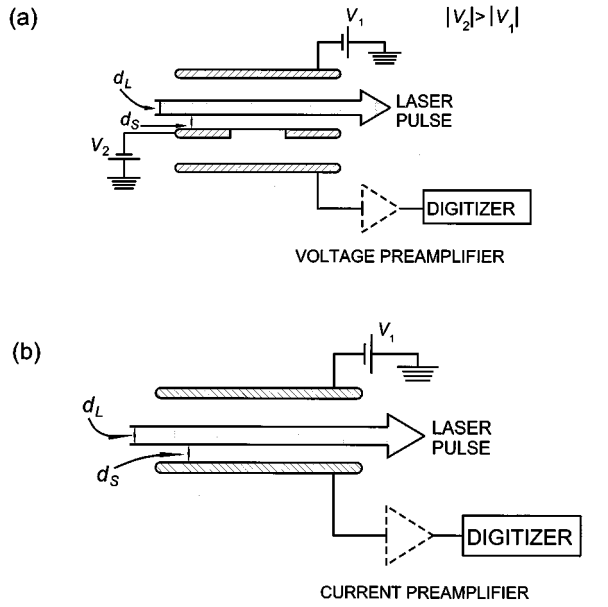

FIG. 2. Schematic diagram of the laser-electrode arrangement for (a) the charge detection mode and (b) the current detection mode. In (a), the electrons and negative ions were extracted to the detection region located between the lower two electrodes and voltages induced by them in that region were monitored. In (b), the current due to the electrons in the interaction region was monitored in real time (currents due to positive and negative ions are negligible).

lifetime of 2 ns [44]. This is also consistent with the production of $H(n=2)$ states via electron attachment to long-lived HR states.

Finally, the relevant rate equations were solved numerically to fit the experimental electron attachment data; this yielded a lower bound for the rate constant for electron attachment to the HR states of $\sim 5\times 10^{-5}$ cm^3 s^{-1}. These findings are discussed and their implications for H^+ formation in H_2 discharge sources are pointed out in Sec. III.

II. EXPERIMENT

In the present studies in addition to the technique used in the previous study [7], we employed another technique [45] to measure electron attachment to ArF-laser irradiated H_2. In order to obtain additional information on the states that are directly or indirectly populated by laser irradiation, fluorescence measurements on laser irradiated H_2, were conducted at the University of Louisville.

We employed two experimental techniques to study electron attachment to laser-excited H_2. In both of these, H_2 at pressures of 5–50 Torr was irradiated by a pulsed ArF laser and the resulting electrons and/or ions were monitored indirectly; of the electrons produced by laser photoionization of H_2, some were attached to excited states of H_2 produced by the same laser pulse to yield negative ions.

In the first technique [46], electrons and negative ions produced by a laser pulse in the interaction region were extracted to a separate detection region through a grid in the middle electrode by applying electric fields in the two regions, see Fig. 2(a): the voltage induced by the electrons and negative ions in the detection gap was measured by using a preamplifier with input impedance of $\sim 10^{11}$ Ω in the detection circuit; the contributions from the electrons and negative ions could be distinguished due to the orders of magnitude difference in their drift velocities giving rise to fast and slow components in the signal wave forms. This mode of operation is called the ''charge detection mode,'' and can be used to determine the number densities of negative ions and electrons that resulted from interactions occurred in the interaction region as a function of the laser intensity.

In the second technique [45], the loss of electrons in the laser-irradiated region due to attachment was monitored in real time by detecting the electron current in the interaction region gap. A negative voltage was applied to one electrode and the electron current in the gap was monitored by connecting the other electrode to a fast digitizer with 50 Ω input impedance, see Fig. 2(b); [in this case only the top two electrodes in Fig. 2(a) were used and the bottom electrode was grounded]. The time constant of this detection circuit was $\sim 10^{-9}$ s and thus the monitored signal was directly proportional to the current carried by the electrons. (Due to the smaller drift velocities associated with the positive and negative ions, their contribution to the monitored current was negligible.) The loss of electrons due to attachment appeared as a reduction in current, and therefore electron attachment was monitored in real time. This mode of operation is called the ''current detection mode.'' Since signal voltages of the order of 1 mV were involved, it was essential to minimize the background noise (especially due to the excimer laser) to very low values.

The closest edge of the laser beam of ''width'' d_L (≈ 0.1 cm) was kept at a distance d_s (≈ 0.1 cm) away from the bottom electrode and parallel to it [see Fig. 2(b)]. A negative voltage was applied to the top electrode so that the negatively charged particles drifted to the bottom electrode. The current due to the electrons was monitored at the bottom electrode (that due to negative and positive ions was negligible). Photoemission at the top electrode due to scattered laser light contributed a small background to the overall signal; this constant background extended to longer times compared to the signal due to the photoionization electrons, and was subtracted. (By the time the photoelectrons reached the laser-irradiated region, the excited molecules with lifetimes <100 ns had already decayed; therefore, those electrons did not contribute to the negative-ion formation.)

A Lambda Physik Lextra-50 excimer laser was used in the electron attachment experiments. The telescoped cross section of the laser beam was ~ 0.1 cm^2 and the ''length'' of the interaction region was ~ 10 cm, i.e., the detected negative ions were produced over a ''volume'' of ~ 1 cm^3. While the electrons produced at the ''top'' of the laser pulse traversed the maximum distance of 0.1 cm ($=d_L$) across the laser-irradiated region, those produced at the ''bottom'' of the laser pulse left the laser-irradiated region immediately, see Fig. 2(b). Therefore, the maximum time an electron spent in the laser-irradiated region was d_L/w_e, where w_e is the drift velocity of the electrons. It is important to note that significant electron attachment did not occur outside the laser-irradiated volume since electron attachment to the lowest-vibrational state H_2 populated at room temperature is extremely weak [1]. Therefore, virtually all negative ions

detected were produced in the laser-irradiated volume.

The fluorescence data were taken with a Questek model 2420 ArF laser. A 15 cm focal length fused silica lens was used to focus the laser pulse to a focal point about 2 cm off of the spectrometer axis, which was perpendicular to the direction of ArF propagation. The average cross-sectional area through the region of observation was 3.6×10^{-2} cm^2, with 175 mJ delivered over a 30 ns pulse. There was no visible breakdown, even at the focal point, under these conditions. A MgF_2 window was used to transmit the fluorescence light to an Acton VM 502 vacuum spectrometer, and the spectra were detected with an EMI type G solar blind photomultiplier. Data were recorded with a Stanford Research Instruments model SR 430 multichannel scaler. The scaler and the spectrometer were automatically controlled by a PC running Linux to acquire a complete temporal profile for one spectral channel on each laser shot. Typically, a sum of 100 shots was recorded as a two-dimensional array with time increments of 5 ns and spectral increments of 5 Å. After acquisition, the database could be reviewed as an image using interactive SAO image display software to give simultaneously the spectrum at every time delay after the laser shot, and the time dependence of every spectral element.

III. RESULTS AND DISCUSSION

A. Electron attachment measurements

As described in Sec. II, measurements in the ''charge detection mode'' allow the number densities of the negative ions and unattached electrons to be estimated. In this mode, the ''fast component'' of the signal voltage V_E was proportional to the number density of the (unattached) electrons that arrived in the detection region; the ''slow component'' of the signal voltage V_I was due to the negative ions. The sum of these two components V_T was proportional to the number density of the electrons initially produced by photoionization; some of these initial electrons were converted to negative ions by electron attachment to excited states produced by the same laser pulse. (By reversing the applied electric fields, positive ions could be extracted to the detection region and then only a slow component that was equal in magnitude to V_T was observed.) For the data presented in this paper, the density of charged species corresponding to a signal level of 100 mV was $\sim10^8$ cm^{-3}.

The laser intensity dependence of the measured V_T and V_I are shown in Figs. 3(a) and 3(b) for 5 and 50 Torr of H_2 at an applied field of 50 V cm^{-1}. At low-laser intensities (I), $V_T=V_E$, but with increasing I the negative-ion signal grew rapidly at the expense of the electron signal, see Fig. 3; at high I, the signal consisted almost entirely of negative ions. For the 5-Torr data in Fig. 3(a), at high laser intensities the negative-ion signal growth became slower due to the unavailability of electrons for attachment, since the negative-ion signal increased faster than electron production by photoionization; thus, the negative-ion signal followed the total signal at these high laser intensities. For 50-Torr data, for which the E/N value (E is the applied electric field and N is the number density of H_2 molecules) was lower, the charge transmission to the detection region became less than unity at high-charge densities [46], and both the V_T and V_I deviated from the initial dependences.

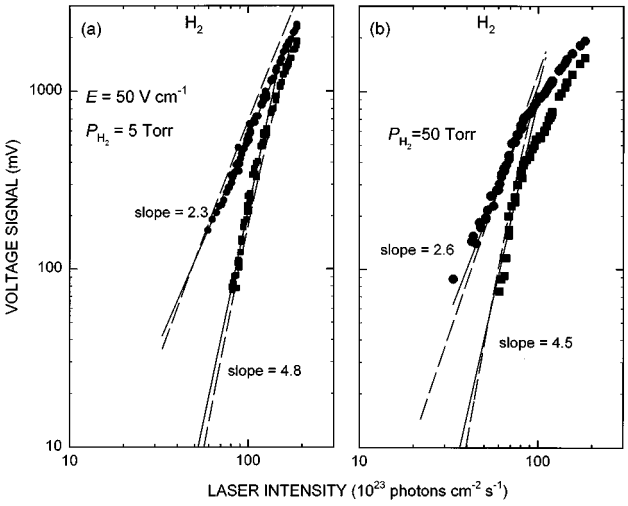

FIG. 3. Laser intensity dependence of the measured total (electrons+negative ions) (●) and negative ion (■) signals for (a) 5 Torr of H_2 pressure and (b) 50 Torr of H_2 pressure. Both sets were taken for an applied electric field of 50 V cm^{-1}. The fitted curves shown by the solid lines were obtained by a least-squares fit (see Sec. III A) to the experimental data. The calculated curves shown by the dashed lines were obtained by numerically solving the relevant rate equations (see Sec. III C).

The total signal shown in Fig. 3 contains a small contribution from photoelectron emission at the cathode by scattered laser light, i.e.,

$$V_T=(V_T)_{\mathrm{PE}}+(V_T)_{\mathrm{PI}}, \tag{8}$$

where $(V_T)_{\mathrm{PE}}$ is the contribution from photoemission at the cathode, and $(V_T)_{\mathrm{PI}}$ is the contribution from photoionization of H_2. Since the photoemission contribution should be linearly dependent on the laser intensity, we fitted the experimental data for V_T by the equation

$$V_T=aI+bI^n. \tag{9}$$

The experimental data for V_I was fitted by the equation

$$V_I=cI^m. \tag{10}$$

Therefore, the n and m values obtained from the above least-squares fittings yielded the laser intensity dependences for laser photoionization and for negative-ion formation. For the data in Fig. 3(a), we obtained $n=2.3$ and $m=4.8$; for the data of Fig. 3(b), we obtained $n=2.6$ and $m=4.5$. Only the ''straight'' sections of the V_T and V_I curves were used for fitting, i.e., data for $I<1\times10^{25}$ cm^{-2} s^{-1} for 5-Torr data, and those for $I<8\times10^{24}$ cm^{-2} s^{-1} for 50-Torr data. The fitted curves are shown by solid lines. It must be noted that the data published in our first report [7] did not make allowance for photoemission, and also the data were not fitted to obtain the laser intensity dependences, i.e., the analysis was too simplified.

Since photoionization of H_2 at the wavelength of the ArF laser (wavelength~193 nm) requires three photons (see Fig. 1), one would expect V_T to increase as I^3. The somewhat smaller power dependence we obtained from the experimental data was due to the efficient photon absorption from the

E,F state. Using a rate equation analysis, it can be shown [18] that the power dependence changes from 3 to 2 if the decay rate of the E,F state due to all other processes (i.e., radiative decay, collisional decay, etc.) is too small compared to the up-pumping rate from the E,F state. In the present case, those two rates are somewhat comparable; the numerical analysis discussed in Sec. III C reproduced the measured power dependences (the dashed curves in Fig. 3).

The observed power dependence for negative-ion formation was about twice that for photoionization. Since each negative ion requires an attaching electron and an excited molecule, this indicates that the excited molecule also originates at the three-photon level, i.e., above the ionization threshold. This is consistent with our contention [43] that electron attaching species are the HR states that are indirectly populated by the SES lying at the three-photon level.

Signal wave forms obtained using the ''current detection mode'' [45] for 50 Torr of H_2 irradiated by an ArF excimer laser are shown in Fig. 4. As described in Sec. II, the current induced by the motion of the electrons in the interaction region gap was recorded in real time using this technique. Figure 4(a) shows a signal wave form at a low-laser intensity, where no significant electron attachment occurred during the drift through the laser-irradiated region; the electron current reached the maximum value over the duration of the laser pulse [laser temporal profile is shown in Fig. 4(d)], and then remained almost constant [region I in Fig. 4(a)] until the electrons from the closest edge of the laser pulse reached the middle electrode in the three-electrode system used in the apparatus [in this case only the top two electrodes were used and the bottom electrode was grounded; only the top two electrodes are shown in Fig. 2(b)]. The linear decay of the current after ~ 125 ns [in region II of Fig. 4(a)] was due to the gradual loss of electrons to the middle electrode. Figure 4(c) shows a signal wave form that resulted when significant attachment of electrons to the excited H_2 molecules as the electrons drifted through the laser-irradiated region; the decrease occurred for ~ 40 ns after the termination of the laser pulse and then the current remained constant during the rest of the drift until the electrons reached the middle electrode. The time over which the electron current decreased during their drift is a *lower limit* to the lifetime of the electron attaching species [45]. Therefore, we can conclude that under the experimental conditions of Fig. 4(b), the lifetime of the electron attaching species must be $\geqslant 40$ ns. When the laser intensity was further increased, electron current decreased rapidly, see Fig. 4(c); this occurred basically within the duration of the laser pulse [see Fig. 4(d)] due to the rapid attachment of electrons to a high-number density of excited states populated at this high laser intensity, i.e., the lifetimes of the attaching species were reduced by electron attachment itself.

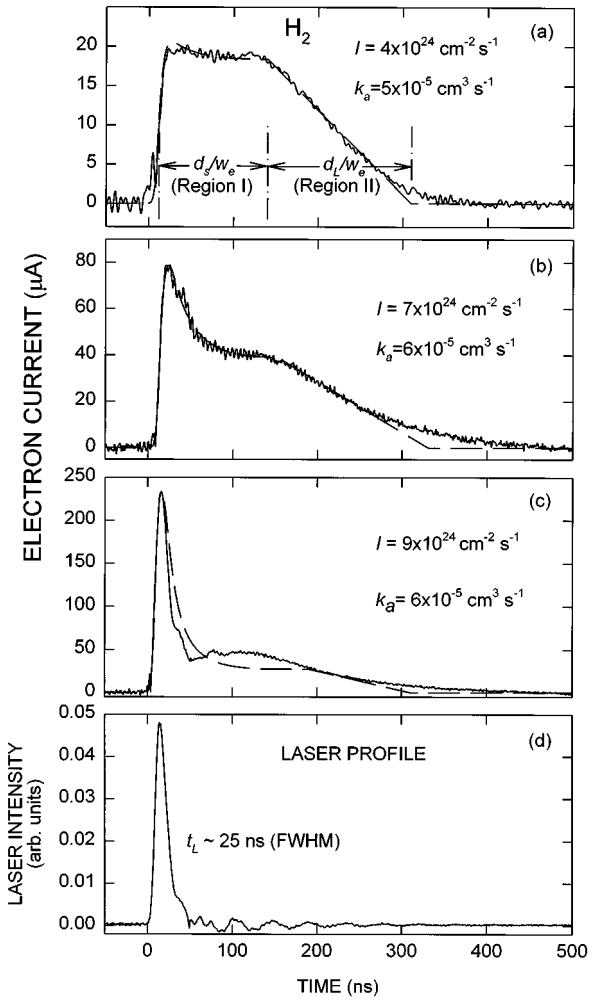

FIG. 4. Signal wave forms in the ''current detection mode'' for the laser intensities indicated in the figure for 50 Torr of H_2 at an applied electric field of 50 V cm^{-1}. In (a), the electron current remained almost constant in region I [also see Fig. 2(b)] since the loss of electrons due to attachment was small. As the laser intensity was increased in (b) and (c), more and more electrons were lost via attachment to excited states. The linear loss of electrons in region II in (a)–(c) was due to the loss of electrons to the lower electrode [see Fig. 2(b)]. The simulated wave forms, obtained by numerically solving the appropriate rate equations (see Sec. III C), are shown by dashed lines. (d) The laser temporal profile. (This is also a ''current detection mode'' wave form, but with a vacuum in the experimental chamber; the electrons were produced at the cathode by scattered laser light.)

B. Fluorescence measurements

The above measurements and the discussion in Sec. I indicate that the electron attaching species are likely to be HR states that are populated indirectly by laser-populated SES states. This was confirmed by the fluorescence measurements presented below.

Molecular emissions at 1600 and 1200 Å in the Lyman and Werner bands, resulting from $B\ ^1\Sigma_u^+ \rightarrow X\ ^1\Sigma_g^+$ and $C\ ^1\Pi_u \rightarrow X\ ^1\Sigma_g^+$ transitions were observed. *Within the duration of the laser pulse*, the intensity for $C \rightarrow X$ emission was ~ 15 times stronger than that for the $B \rightarrow X$ emission after correcting for system response. This is consistent with the proposition of Kligler, Boker, and Rhodes [18] that the collisional quenching of the E,F state occurs by population transfer to the $C(v=2)$ state. The spectrum is also consistent with this model. There is strong emission at 1180, 1220, and 1260 Å as would be expected. The observed intensity ratios are also consistent with significant emission only originating in $C\ ^1\Pi_u(v=2)$ when allowance is made for the diminished transmission of the MgF_2 window at the short wavelength limit. Since emission from $C\ ^1\Pi_u(v=0,1)$ also occurs in the

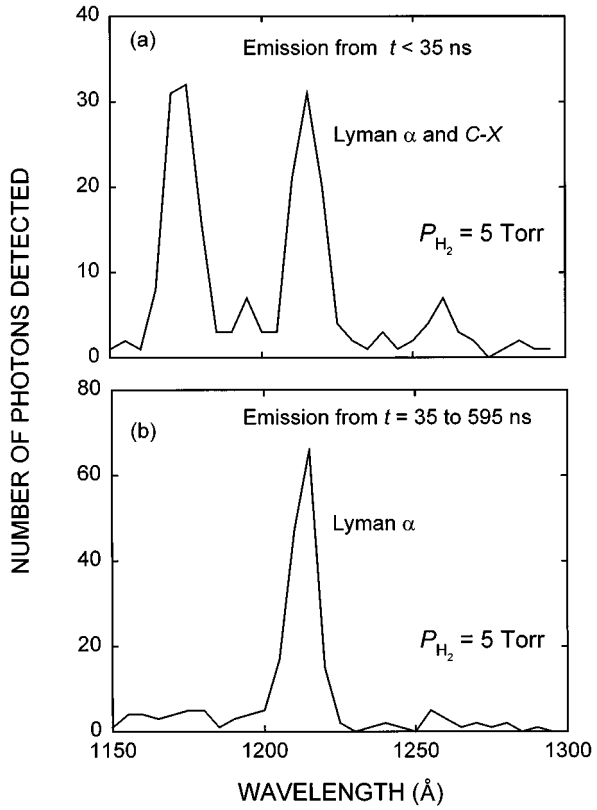

FIG. 5. Observed fluorescence spectrum in the 1100–1300 Å region with light monitored for (a) 0–35 ns, i.e., within the duration of the laser pulse, and (b) from 35–195 ns, i.e., after the laser was turned off. The light was collected in 5-ns time bins. While *C-X* emission dominates the spectrum within the duration of the laser pulse, it is weak after the laser was turned off. The narrow spike at 121.5 nm in (b) is due to Lyman α, which is ''hidden'' in the *C-X* emission at 121.7 nm in (a).

same regions at our spectral resolution, we cannot determine exactly the fraction that might also arise from these states, but it is small compared to that from $v=2$. A complete analysis was possible for $B\rightarrow X$ emission, and the lifetime measurements were obtained for both $B\rightarrow X$ and $C\rightarrow X$ emissions. *After the termination of the laser pulse, B-X* emission persisted for long times up to 100 ns; even though the *C-X* emission could also be seen it was much weaker than the *B-X* emission at these long times.

We also observed Lyman-α emission at 1215 Å due to $n=2$ to $n=1$ transitions in atomic hydrogen. To our knowledge, this has not been reported previously for two-photon excitation to $E,F\ ^1\Sigma_g^+$ state. This narrow emission line is located in the *C-X* emission region, but its temporal signature is quite different from the *C-X* molecular emission. The observed spectra in this region at different time scales are shown in Fig. 5. It is quite clear that after the laser is turned off (>35 ns), the emission is predominantly due to the Lyman-α line. The *C-X* emission after the laser was turned off was much weaker. Thus, the *C* state was mainly populated during the laser pulse by neutral collisions with the laser-populated E,F $(v=6)$ state.

If the emissions are from the *B* and *C* states that were populated by the directly populated E,F states, then the emissions should basically follow the laser profile since none of the states involved (i.e., the E,F state and the *B* and *C* state) can hold their populations for more than 3 ns (this upper limit is set by the E,F state whose lifetime is reduced to 3 ns at 5-Torr pressure and 0.3 ns at 50-Torr pressure; the *B* and *C* states have sub-ns radiative lifetimes, see Sec. I). The late emissions from the *B* (and to a lesser extent *C*) states thus indicate that they are populated from a higher-lying, long-lived reservoir, most likely they are populated by cascades from high Rydberg states that are known to have comparatively long lifetimes sometimes up to μs range [42]. A similar argument holds for Lyman-α emission. The $H(n=2)$ state has a radiative lifetime of 2 ns. Hence in order for the emission to persist for 100 ns, the $H(n=2)$ state must be generated continuously over that time. We believe that the $n=2$ state of atomic hydrogen is produced in the H formation process of electron attachment to HR states of molecular hydrogen, see Eq. (7).

Furthermore, even within the laser pulse duration, the emission wavelengths profile for the *B-X* emission does not match the spectral profile that can be calculated [47] assuming that the emitting vibrational states of the *B* state are populated by cascades from the E,F Eqs. (6,7) states directly populated by the laser. We modeled this by using the theoretical $E,F\rightarrow B$ transition probabilities [48] to compute the branching ratios to the different vibrational states of $B\ ^1\Sigma_u^+$. The spectrum was then modeled with H2SPEC, a H_2 molecular emission spectral code [47]. For this purpose we assumed a thermal rotational distribution, and a spectral bandwidth equal to that of the spectrometer. These comparisons are shown in Fig. 6(a). The expected spectrum for transitions originating from the initially pumped $E,F(v=6,7)$ levels was obtained by adding the transition probabilities from the $E,F(v=6)$ [i.e., $v_E=2$ state in the *E* well] and $E,F(v=7)$ [i.e., $v_F=4$ state in the *F* well] levels. While the E,F Eqs. (6,7) cascade fluorescence is expected to spread over the entire wavelength region in the figure, the observed spectrum is restricted to the longer wavelengths.

On the other hand, the spectrum that is calculated assuming that the emitting vibrational states are populated by cascades from higher-lying (HR) states agrees well with the observed profile, see Fig. 6(b). For this calculation we assumed that the HR states have *u* symmetry, since they are three-photon excitations from the $X\ ^1\Sigma_g^+$ ground state. (If collisions play a role in stabilizing the HR states, there may be a population of *g*-symmetry states as well.) In order for the molecules to radiate from the $B\ ^1\Sigma_u^+$ state, there must be an intermediate state in the cascade. We assume a process such as

$$H_2(\mathrm{HR})\rightarrow H_2(E,F)\rightarrow H_2(B), \tag{11}$$

where the first step is by electric dipole radiation, and the second by collision. Since the HR states are formed at an internuclear separation, $R\sim 2.4$ Å [12] (via the SES), the favored Franck-Condon factors will lead to large populations in the lowest states of the *F* well. We estimated branching for collisional transfer from F $(v=0,1)$ by weighing with the Franck-Condon factors for the overlap with $B\ ^1\Sigma_u^+$ of various v [49]. While this is only a first approximation to what is clearly a complex process, the agreement with the observed *B-X* emission in Fig. 6(b) is striking.

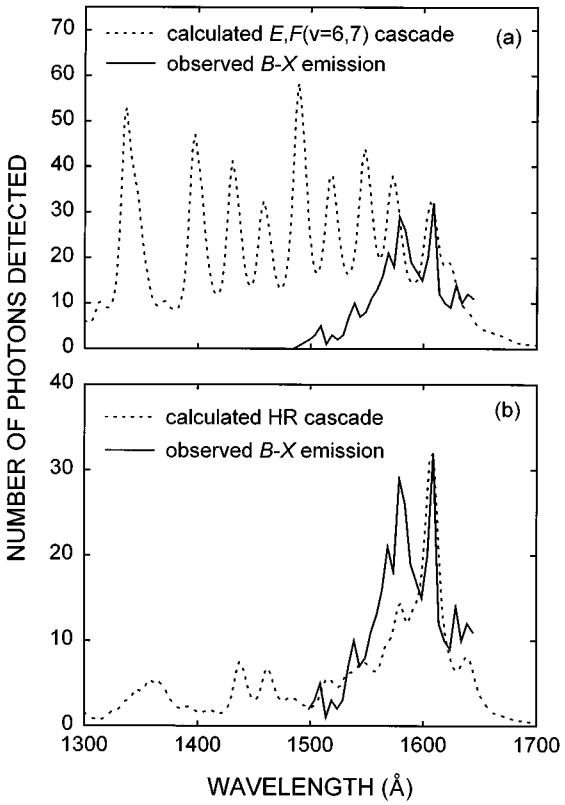

FIG. 6. Comparison of the measured B-X fluorescence spectrum (full lines) with the calculated spectra (dotted lines) for (a) cascades from the initially laser populated E,F (6,7) levels and (b) cascades from high-lying (HR) states that predominantly go through the lowest two vibrational levels in the F well [or E,F (1,2) levels].

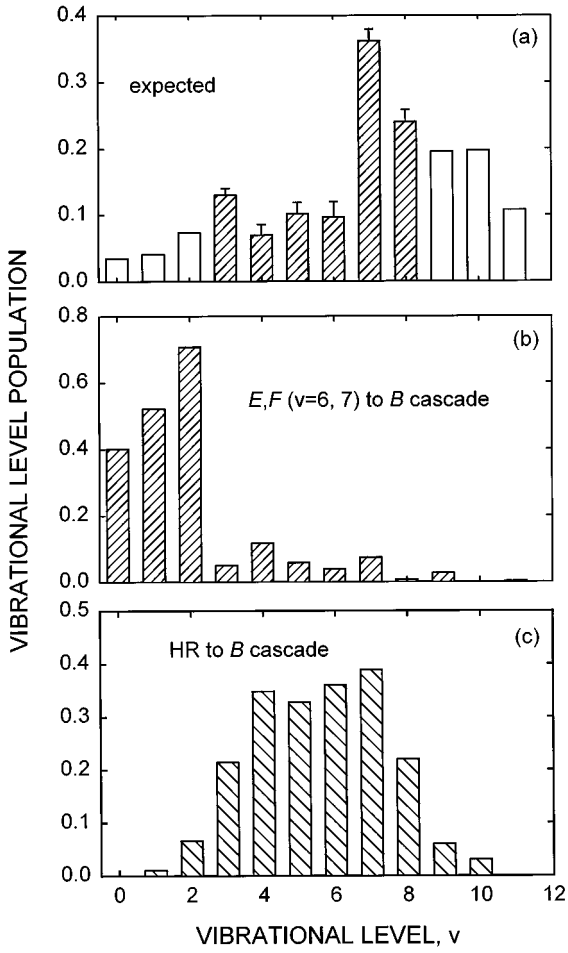

FIG. 7. (a) B-state vibrational distribution needed to match the observed spectrum in Fig. 6. The emission wavelength range was not sufficient to accurately determine the populations of the $v=0-2$ and 9–11 levels, and the maximum possible populations at these are indicated. (b) B-state vibrational state populations calculated for collisional and radiative transitions arising only from the initially populated E,F (6,7) levels. (c) B-state vibrational populations estimated for cascades from the HR states.

The B-state vibrational distribution that fits the observed spectrum is shown in Fig. 7(a). The B-state vibrational distribution expected for collisional and radiative cascades from the laser-populated E and F levels is shown in Fig. 7(b), and that for the HR fitting in Fig. 6(b) is shown in Fig. 7(c). It is clear that the cascades from the laser-populated E,F (6,7) levels are not responsible for the observed emission; the vibrational populations roughly estimated to be due to HR cascades are in fairly good agreement.

The measured spectrum shown in Figs. 6(a) and 6(b) were integrated only for the duration of the laser pulse. Thus even within the duration of the laser pulse, the B-X emission does not originate from the laser-populated E,F (6,7) levels, and cascades from HR states predominate. This is consistent with our contention that up-pumping from the E,F levels is quite efficient, and is predominated by the transitions originating from the F well that lead to population of the HR states via SES.

The fluorescence signal versus time measurements for the $B\rightarrow X$ and Lyman-α emissions are shown in Fig. 8 for 5 and 50 Torr of H_2 and at a fixed laser intensity. At 5 Torr of H_2 pressure, both emissions extend to times well after the termination of the laser pulse and have decay times of $\sim$100 ns. When the H_2 pressure was increased to 50 Torr at the same laser intensity, the decay times for both emissions reduced to 10 ns after the termination of the laser pulse.

The above pressure dependences of the temporal profiles of the molecular and atomic emissions are consistent with the proposed electron attachment mechanism: The observed temporal profiles indicate the effective lifetimes of the HR states. For a given laser intensity, the number density N_{HR} of the HR states is smaller at a low pressure. This lengthens the effective electron attachment time [$=1/(N_{\mathrm{HR}}k_a)$, where k_a is the electron attachment rate constant]. Since the B state is populated by cascades from the HR states, the B-X emission continues to $\sim$100 ns after the ArF pulse, see Fig. 8(a). Furthermore, attachment of electrons to the HR states [see Eq. (7)] produces H($n=2$) atoms that gives rise to Lyman-α emission over the effective lifetime of the HR states of $\sim$100 ns, see Fig. 8(c). (The estimated lifetime for the HR states from the electron attachment measurements in the ''current detection mode'' is $\geqslant$40 ns, see Sec. III A; this discrepancy could be due to the different experimental conditions under which the spectroscopic and electron attach-

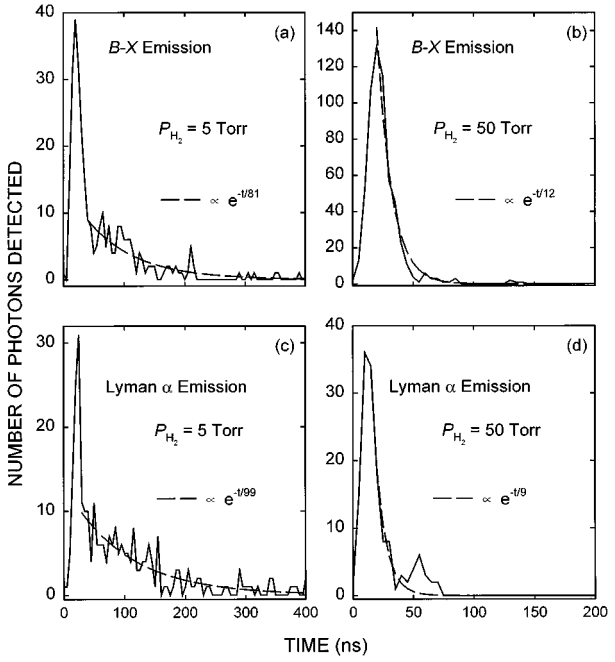

FIG. 8. (a) and (b) Time dependence of the B-X emission at 5 and 50 Torr, respectively; (c) and (d) time dependence of the Lyman-α emission at 5 and 50 Torr, respectively. The laser intensity was kept the same for all four sets of data.

ment measurements were carried out at two different locations.) When the pressure is increased to 50 Torr (keeping the laser intensity the same), the effective lifetimes of the HR states is reduced by electron attachment itself to $\sim$10 ns, and correspondingly, the B-X and Lyman-α emission times are also decreased to $\sim$10 ns [Figs. 8(b) and 8(d)].

Yet another clue was obtained by estimating the number of Lyman-α photons emitted corresponding to the above data at 5 and 50 Torr. Allowance has to be made for the inefficient collection of photons by the small aperture of the spectrometer slit, but the geometry, grating efficiency, and photomultiplier response are well characterized. It is apparent that the number of Lyman-α photons produced per laser shot is of the same order of magnitude as the number of H^- ions formed for corresponding experimental parameters. This correlation is also consistent with our proposed electron attachment process Eq. (7), that is, one Lyman-α photon is emitted for each H^- ion formed.

C. Electron attachment model

The excitation of HR states of H_2 by ArF laser proceeds by Eqs. (1), (3), and (6d); the proposed electron attachment process is given in Eq. (7). The relevant rate equations for the population of the HR states, electron production by photoionization, and negative-ion formation by attachment of those electrons to the HR states can be written as

$$\frac{dN_{E,F}}{dt}=N_0\sigma_e^{(2)}I^2-N_{E,F}(\sigma_e+\sigma_i)I-N_{E,F}\left(\frac{1}{\tau_c^E}+\frac{1}{\tau_r^E}\right), \tag{12}$$

$$\frac{dN_{\rm SES}}{dt}=N_{E,F}\sigma_e I-\frac{N_{\rm SES}}{\tau_{\rm SES}}, \tag{13}$$

$$\frac{dN_{\rm HR}}{dt}=\eta\,\frac{N_{\rm SES}}{\tau_{\rm SES}}-k_a\left(1-\frac{t}{t_L}\right)N_eN_{\rm HR}-\frac{N_{\rm HR}}{\tau_{\rm HR}}, \tag{14}$$

$$\frac{dN_i}{dt}=\left(1-\frac{t}{t_L}\right)(k_aN_{\rm HR})N_e, \tag{15}$$

$$\frac{dN_e}{dt}=N_{E,F}\sigma_i I-\left(1-\frac{t}{t_L}\right)(k_aN_{\rm HR})N_e, \tag{16}$$

where N_0 is the number density of the ground-state H_2 molecules, I is the laser intensity, $N_{E,F}$ is the number density of the E,F state; $N_{\rm SES}$, $N_{\rm HR}$, N_e, and N_i are, respectively, the number densities of the SES, HR states, electrons, and negative ions; $\sigma_e^{(2)}$ is the two-photon absorption cross section for the ground state, σ_i is the total ionization cross section for the E,F state, σ_e is the photoexcitation cross section for the E,F state, τ_r^E and τ_c^E are the radiative and collisional lifetimes of the E,F state respectively; $\tau_{\rm SES}$ is the lifetime of the SES; η is the quantum yield for HR formation from the SES, which was assumed to be 1 in the calculation; $\tau_{\rm HR}$ is the lifetime of the HR states; k_a is the electron attachment rate constants for the HR states, and t_L is the maximum time an electron spends inside the laser irradiated region, see Sec. II.

The above rate equations were solved numerically (also see [45]) to obtain the time development of the various species (excited states, electrons, and negative ions). The following values were used for the various parameters: $\sigma_e^{(2)}=1.2\times10^{-47}$ cm^4 s^{-1} [13]; $\tau_r^E=100$ ns [18–20]; $\tau_c^E=15/(P_{H_2})$ ns, where P_{H_2} is the pressure of H_2 [18,19]; $\tau_{\rm SES}=10^{-14}$ s [32]; $\tau_{\rm HR}=40$ ns; $t_L=40$, 100, and 200 ns for the data at 5, 25, and 50 Torr for all of which the applied electric field was kept at 50 Vcm^{-1}, (the values for $\tau_{\rm HR}$ and t_L were deduced from the ''current detection mode'' wave forms such as those in Fig. 4).

Time evolutions of $N_{E,F}$, $N_{\rm SES}$, $N_{\rm HR}$, N_e, and N_i calculated from numerically solving the above rate equations for a fixed laser intensity are shown in Fig. 9. The values of $N_T=N_e+N_i$ and N_e at $t\rightarrow200$ ns are proportional to the experimentally measured V_T and V_I. Using a proportionality constant of 10^{-6} (i.e., the measured signal in mV correspond to the calculated number density times 10^{-6}), the V_T and V_I values were calculated for a given laser intensity. The values for σ_e and σ_i were adjusted so that our ''charge detection mode'' data (such as those in Fig. 3) could be reproduced for the data sets at H_2 pressures of 5, 25, and 50 Torr; the calculated curves for V_T and V_I are shown in dashed lines in Fig. 3 for the 5- and 50-Torr data sets. The best fits were obtained for $\sigma_e=4\times10^{-17}$ cm^2 and $\sigma_i=1.8\times10^{-20}$ cm^2. The k_a values were slightly adjusted to obtain best fits for V_I curves at different H_2 pressures; for the 5-, 25-, and 50-

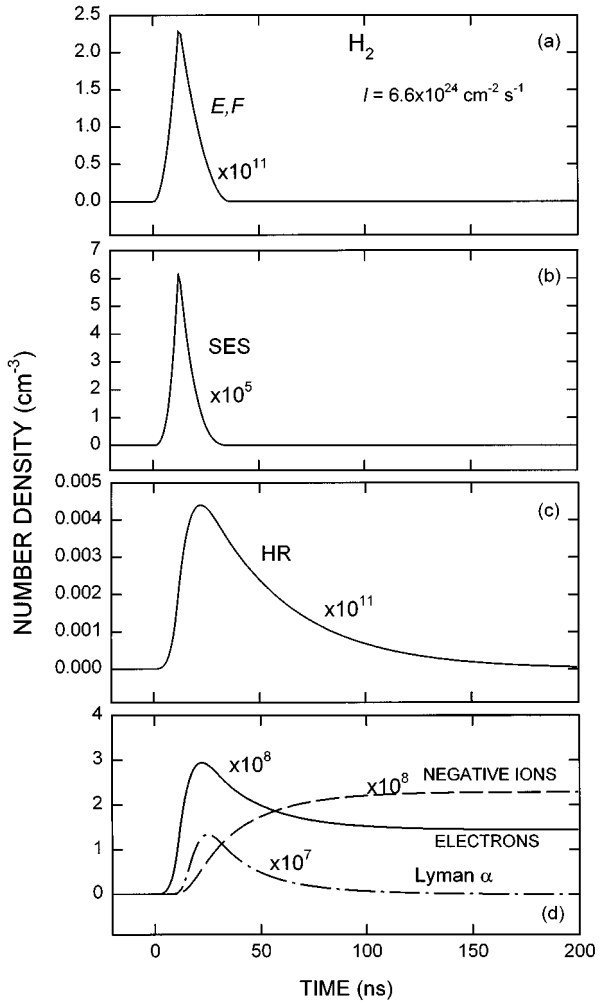

FIG. 9. Calculated time evolution of the number densities of (a) the E,F state, (b) SES, (c) HR states, and (d) electrons, Lyman-α photons, and negative ions for experimental parameters corresponding to Fig. 3(b). The numbers on the Y axis need to be multiplied by the factors given inside the plots. Note that the number of Lyman-α photons emitted is given by the area under the curve.

Torr data sets, the ''best values'' for k_a were 4.5×10^{-5}, 6×10^{-5}, and 8.8×10^{-5} cm^3 s^{-1}. Thus the estimated k_a value is $\sim6\times10^{-5}$ cm^3 s^{-1}, which roughly translates into a cross section of the order of 10^{-10} cm^2. It must be noted that this is a lower bound for the actual value since it was assumed that the SES are converted to HR states with unit efficiency [i.e., η in Eq. (14) was assumed to be 1].

In the above calculations, the 40-ns lifetime for HR states estimated from the ''current mode wave forms'' was used; if we used the 100-ns lifetime estimated from the spectroscopic measurements, then electron attachment rate constant values of about a factor of 2 lower were needed, but the shape of the simulated ''current mode'' wave forms did not match well with the experimental ones.

High Rydberg states of atoms and molecules are known to have extremely large cross sections for interaction with charged particles and cross sections of this magnitude are not uncommon (for example, see pp. 240 and 330 of [42] and [50]). In the present case, the electron attachment process of Eq. (7) occurs by a two-step process

$$H_2^*(HR)+e^- \xrightarrow{\sigma_c} H_2^{-**} \xrightarrow{p} H^- + H(n=2), \qquad (17)$$

where H_2^{-**} is a transient negative ion initially produced by the capture of the electron by the excited molecule with a cross section, σ_c; this transient state stabilizes by dissociating into the ionic and neutral fragments with a probability p. The initial capture cross section (σ_c) is generally large for excited states due to their high polarizabilities. The polarizability of a Rydberg state increases as n^7, where n is the principal quantum number. Even though polarizabilities of molecular Rydberg states have not been reported to our knowledge, enormous polarizabilities of $>10^9$ Å^3 were reported for Rydberg states of Cs [51]. Now, the transient negative-ion state is likely to rapidly dissociate with a high probability (p) due to its large internal energy content. Thus the actual electron attachment cross section, σ_a, given by

$$\sigma_a = \sigma_c p \qquad (18)$$

could be very large. We have observed similarly large cross sections for electron attachment to several other molecules excited to energies above their ionization thresholds by both resonant [46,52] and nonresonant [53,54] laser excitation processes; in the latter case (for silane [53] and methane [54]) in particular, electron attachment to HR states indirectly populated by SES are quite likely to be the electron attachers since no bound excited states were directly populated by the laser. In both these molecules, the first electronically excited singlet state lies above the photon energy of the laser and the molecule is ionized by absorption of two photons. Further studies on these two molecules are in progress.

A cross section of the order of 10^{-10} cm^2 is of the same order of magnitude as the geometric cross section of a $n\sim25$ Rydberg state, which should have radiative lifetimes of the order of microseconds; this is long compared to our measured lifetimes of the order of 100 ns. However, while some cross sections associated with Rydberg states are of the order of geometric cross sections, there are other cross sections that are larger than the geometric cross sections; for example, l-changing cross sections can vary as n^5 [55]. Thus, the states responsible for an electron attachment rate constant of the order of 10^{-10} cm^2 do not necessarily have to be Rydberg states of $n\sim25$. In particular, for electron collisions with Rydberg states, the initial capture cross section may vary as n^7 due to the role played by the polarizability, see above. Another factor to be considered is the effect of the ambient pressure on the lifetimes of the Rydberg states. Thus with the present experiments it is not possible to estimate the n values of the Rydberg states responsible for the observed electron attachment. Experiments are being planned to conduct electron attachment measurements on well-defined Rydberg states directly populated under single collision conditions.

In the present experiment, high-vibrational (HV) states of the ground-electronic state are populated by the B-X and C-X transitions; to estimate an absolute lower limit for attachment to these HV states needed to produce the experimentally observed negative-ion number densities, we nu-

merically solved the appropriate rate equations optimized for that process, i.e., we set the parameters so that all the molecules pumped to the E,F state will end up in the high-v states ($v>8$) of $X\ ^1\Sigma_g^+$ state (which are supposed to have the highest rate constant for electron attachment) except for the loss of E,F state by ionization, i.e., $\sigma_i=1.8\times10^{-20}$ cm^2, and $\sigma_e=0$. We obtained a required rate constant of $\sim10^{-6}$ cm^3 s^{-1} as was estimated by a back-of-the-envelope type calculation made previously Eq. [7]; as we emphasized above this would be an absolute lower limit for the required rate constant. Yet, the maximum electron attachment rate constant associated with the HV states is predicted to be 10^{-8} cm^3 s^{-1} [4,5], more than two orders of magnitude smaller than the required rate constant. Thus the contribution to the observed H^- signal from the HV states in our experiments should be less than 1%.

D. Upward transitions from the E,F state

In Sec. II C above, we estimated an ionization cross section, σ_i, of $\sim1.8\times10^{-20}$ cm^2 and an excitation cross section, σ_c, of $\sim4\times10^{-17}$ cm^2 for the upward transitions from the E,F state; the excitations are associated with populations of the SES, see Fig. 1. None of the previous experiments [13,18] that estimated the ionization cross section of the E,F state had monitored the photoionization signal directly; in both those experiments [13,18] only the near-infrared emission due to the $E,F\ ^1\Sigma_g^+\rightarrow B\ ^1\Sigma_u^+$ transition was monitored.

(i) Kligler, Bokor, and Rhodes [18] had observed the near-infrared $E,F\ ^1\Sigma_g^+\rightarrow B\ ^1\Sigma_u^+$ emission from ArF-laser irradiated H_2: By conducting a rate equation analysis for the dependence of IR intensity on H_2 pressure, they estimated [18] the photoabsorption cross section of the E,F state to be between 8×10^{-19} and 4×10^{-18} cm^2. This estimated cross section was reported [18] as the ionization cross section for the E,F state; in other words, they associated all upward transitions originating from the E,F state with molecular ionization.

(ii) Buck *et al.* [13] measured the excited-state absorption cross section by conducting pump-probe experiments, where the $E,F\ ^1\Sigma_g^+\rightarrow B\ ^1\Sigma_u^+$ near-IR emission due to the pump laser was quenched by upward transitions from the E,F state due to the probe laser. A value of $\sim6.4\times10^{-18}$ cm^2 was estimated for the absorption cross section ($=\sigma_i+\sigma_c$).

Buck *et al.* [13] also calculated the absorption cross section for the E,F state at the ArF line, which included direct photoionization and excitation of only one of the SES that are accessible from the F well. Based on the work of Cohn [56], the cross section for direct photoionization from the E state was estimated by Buck *et al.* [13] to be $\sim3\times10^{-18}$ cm^2 (a more recent calculation by Rudolph *et al.* [57] was shown to yield about 25% smaller value [13]); the cross section for excitation of the $^1\Sigma_u^+$ $(2p\sigma_u2s\sigma_g)$ doubly excited state was calculated to be $\sim8\times10^{-18}$ cm^2 [13], thus giving an estimated total absorption cross section of $\sim11\times10^{-18}$ cm^2 [13]. However, it appears that transitions to the other doubly excited SES (see Fig. 1) were not taken into account, which would have made the estimation of the total absorption cross section even higher; we estimate a total absorption cross section of $\sim4\times10^{-17}$ cm^2, see Sec. III C.

Therefore, to our knowledge, no prior experiment had directly measured the photoionization signal. Calculations of Cohn [56] and Rudolph *et al.* [57] yield direct photoionization cross section of the order of 10^{-18} cm^2 for *excitations from the E well of the E,F state*. This value is two orders of magnitude larger than the value we estimate for effective photoionization cross section from the E,F state. It must be emphasized that under our experimental conditions, population of the E well is depleted rapidly via excitation transfer to C state and also to the F well; upward transitions from the F well mostly result in the excitation of the SES rather than direct ionization.

In order to verify our estimated cross sections, we measured the total signal in the ''charge detection mode'' (see Secs. II and III) at a H_2 pressure of 0.5 Torr, the experimental curve for photoionization versus laser intensity was obtained by correcting for photoemission at the cathode due to scattered laser light, see Sec. III. This experimental curve was reproduced to an accuracy comparable to those in Fig. 3 by the numerical code with the same parameters used for 5 and 50 Torr data of Fig. 3. Thus the estimates of the ionization cross section and the absorption cross section were consistent with our data for H_2 pressures over two orders of magnitude.

IV. SUMMARY

Comprehensive electron attachment and spectroscopic measurements were carried out on ArF-laser irradiated H_2. These measurements are consistent with an efficient electron attachment process involving highly excited Rydberg (HR) states of H_2 indirectly populated via laser irradiation. The electron attachment measurements indicated a lifetime of $\geqslant40$ ns for the electron attaching species. Under our experimental conditions all low-lying electronically excited states that may be produced directly or indirectly via laser irradiation have lifetimes at least an order of magnitude smaller; the HV states of the ground electronic state that may be populated indirectly would have too long lifetimes.

The Lyman-α emission observed was shown to be consistent with $H(n=2)$ state produced via electron attachment to HR states with energies >14 eV. The ''late emission'' in the B-X emission region that persists up to 100 ns after the laser pulse was shown to be consistent with the population of B vibrational states via cascades from HR states. However, fundamental questions remain to be answered as to how the initially excited SES can be converted to HR states prior to the destruction of the SES by preionization and/or predissociation.

ACKNOWLEDGMENTS

The work of L.A.P. and P.G.D. was supported by the National Science Foundation under Contracts Nos. CHE-9313949 and ECS-9626217 with the University of Tennessee, Knoxville, and by the LDRD Program of the Oak Ridge National Laboratory, managed by Lockheed Martin Energy Research Corp. for the U.S. Department of Energy under Contract No. DE-AC05-96OR22464. The work by J.F.K. was supported by the Division of Chemical Sciences, Office of Basic Energy Sciences, U.S. Department of Energy.

[1] G. J. Schulz and R. K. Asundi, Phys. Rev. **158**, 25 (1967).
[2] M. Allan and S. F. Wong, Phys. Rev. Lett. **41**, 1791 (1978).
[3] J. M. Wadehra and J. N. Bardsley, Phys. Rev. Lett. **41**, 1795 (1978).
[4] J. M. Wadehra, Phys. Rev. A **29**, 106 (1984).
[5] A. P. Hickman, Phys. Rev. A **43**, 3495 (1991).
[6] C. Bottcher and B. D. Buckley, J. Phys. B **12**, L497 (1979).
[7] L. A. Pinnaduwage and L. G. Christophorou, Phys. Rev. Lett. **70**, 754 (1993).
[8] L. A. Pinnaduwage and L. G. Christophorou, J. Appl. Phys. **76**, 46 (1994).
[9] J. F. Kielkopf, J. Opt. Soc. Am. B **8**, 212 (1991).
[10] J. F. Kielkopf, L. A. Pinnaduwage, and L. G. Christophorou, Phys. Rev. A **49**, 2675 (1994).
[11] T. E. Sharp, At. Data **2**, 119 (1971).
[12] S. L. Guberman, J. Chem. Phys. **78**, 1404 (1983).
[13] J. D. Buck *et al.*, Phys. Rev. A **39**, 3932 (1989).
[14] W. M. Huo and R. L. Jaffe, Chem. Phys. Lett. **101**, 463 (1983).
[15] E. E. Marinero, R. Vasudev, and R. N. Zare, J. Chem. Phys. **78**, 692 (1983).
[16] P. Senn, P. Quadrelli, and K. Dressler, J. Chem. Phys. **83**, 962 (1985).
[17] P. Senn and K. Dressler, J. Chem. Phys. **87**, 1205 (1987).
[18] D. J. Kligler, J. Bokor, and C. K. Rhodes, Phys. Rev. A **21**, 607 (1980).
[19] D. J. Kligler and C. K. Rhodes, Phys. Rev. Lett. **40**, 309 (1978).
[20] D. W. Chandler and L. R. Thorne, J. Chem. Phys. **85**, 1733 (1986).
[21] H. Pummer, H. Egger, T. S. Luk, T. Srinivasan, and C. K. Rhodes, Phys. Rev. A **28**, 795 (1983).
[22] U. Czarnetzki, H. F. Dobele, and B. Ruckle, Appl. Phys. B **48**, 37 (1989).
[23] L. Spitzer and J. L. Greenstein, Astrophys. J. **114**, 407 (1951).
[24] E. M. Purcell, Astrophys. J. **116**, 457 (1952).
[25] J. E. Hesser, J. Chem. Phys. **48**, 2518 (1968).
[26] H. Schmoranzer and J. Imschweiler, Phys. Lett. **100A**, 85 (1984).
[27] J. H. Kieffer and R. W. Lutz, J. Chem. Phys. **44**, 668 (1966).
[28] W. S. Barnes, D. W. Martin, and E. W. McDaniel, Phys. Rev. Lett. **6**, 110 (1961).
[29] A. V. Phelps, J. Phys. Chem. Ref. Data **19**, 653 (1990).
[30] B. Peart and K. T. Dolder, J. Phys. B **8**, 1570 (1975).
[31] B. Peart, R. A. Forrest, and K. Dolder, J. Phys. B **12**, 3441 (1979).
[32] J. Tennyson and C. J. Noble, J. Phys. B **18**, 155 (1985).
[33] S. T. Pratt, E. F. McCormack, J. L. Dehmer, and P. M. Dehmer, Phys. Rev. Lett. **68**, 584 (1992).
[34] S. T. Pratt (private communication).
[35] M. Ciocca, M. Allegrini, E. Arimondo, C. E. Burkhardt, W. P. Graves, and J. J. Laventhal, Phys. Rev. Lett. **56**, 704 (1986).
[36] L. M. Branscomb, in *Photodetachment, in Atomic and Molecular Processes*, edited by D. R. Bates (Academic, New York, 1962), p. 100.
[37] K. P. Huber and G. Herzberg, *Constants of Diatomic Molecules* (Van Nostrand Reinhold, New York, 1979).
[38] W. Chupka, J. Chem. Phys. **87**, 1488 (1987).
[39] W. A. Chupka, P. J. Miller, and E. E. Eyler, J. Chem. Phys. **88**, 3032 (1988).
[40] T. Bear, P. M. Guyon, I. Nenner, A. Tabche-Fouhaille, R. Botter, L. F. A. Ferreira, and T. R. Graves, J. Chem. Phys. **70**, 1585 (1979).
[41] P. M. Guyon, T. Bear, and I. Nenner, J. Chem. Phys. **78**, 3665 (1983).
[42] R. F. Stebbings and F. B. Dunning, *Rydberg States of Atoms and Molecules* (Cambridge University Press, Cambridge, 1983).
[43] L. A. Pinnaduwage, in *Proceedings of the Seventh International Symposium on Production and Neutralization of Negative Ions and Beams and the Sixth European Workshop on Production and Application of Light Negative Ions*, edited by K. Prelec (AIP, New York, 1996), pp. 44–60.
[44] E. U. Condon and G. H. Shortley, *The Theory of Atomic Spectra* (Cambridge University Press, Cambridge, 1964), p. 137.
[45] L. A. Pinnaduwage and P. G. Datskos, J. Chem. Phys. **104**, 8382 (1996).
[46] L. A. Pinnaduwage, L. G. Christophorou, and A. P. Bitouni, J. Chem. Phys. **95**, 274 (1991).
[47] J. Kielkopf, K. Myneni, and F. Tomkins, J. Phys. B **23**, 251 (1990).
[48] M. Glass-Maujean, P. Quadrelli, and K. Dressler, At. Data Nucl. Data Tables **30**, 273 (1984).
[49] C. S. Lin, J. Chem. Phys. **60**, 4660 (1974).
[50] G. W. Foltz, E. J. Beiting, T. H. Jeys, K. A. Smith, F. B. Dunning, and R. F. Stebbings, Phys. Rev. A **25**, 187 (1982).
[51] A. F. J. van Raan, G. Baum, and W. Raith, J. Phys. B **9**, L349 (1976).
[52] L. A. Pinnaduwage and L. G. Christophorou, Chem. Phys. Lett. **186**, 4 (1991).
[53] L. A. Pinnaduwage, M. Z. Martin, and L. G. Christophorou, Appl. Phys. Lett. **65**, 2671 (1994).
[54] L. A. Pinnaduwage, M. Z. Martin, and L. G. Christophorou, Contrib. Plasma Phys. **35**, 433 (1995).
[55] K. B. MacAdam, D. A. Crosby, and R. Rolfes, Phys. Rev. Lett. **44**, 980 (1980).
[56] A. Cohn, J. Chem. Phys. **57**, 2456 (1972).
[57] H. Rudolph, D. L. Lynch, S. N. Dixit, V. McKoy, and W. M. Huo, J. Chem. Phys. **86**, 1748 (1987).